DOI: 10.1002/ejic.200600860

The Effect of Hydrothermal and Non-Hydrothermal Synthesis on the Formation of Holmium(III) Succinate Hydrate Frameworks

Maria C. Bernini,[a] Elena V. Brusau,[a] Griselda E. Narda,*[a] Gustavo E. Echeverria,[b,c] C. Gustavo Pozzi,[b] Graciela Punte,[b] and Christian W. Lehmann[d]

Keywords: Lanthanides / Hydrothermal synthesis / Hybrid frameworks / Coordination polymers

Two novel hydrated holmium(III) succinates with formula $[Ho_2(C_4H_4O_4)_3(H_2O)_4]\cdot 6H_2O$ (**1**) and $[Ho_2(C_4H_4O_4)_3(H_2O)_2]\cdot H_2O$ (**2**) have been synthesized from aqueous solution under ambient and hydrothermal conditions, respectively. Single-crystal X-ray diffraction shows that Ho^{III} is nine-coordinate in both compounds even though their structures are markedly different, the main distinctive features being the $[H_2O]/[C_4H_4O_4^{2-}]$ ratio in the coordination sphere, the conformation and coordination ability of the succinate ions, and the resulting framework dimensionality. Compound **1** is a 2D hybrid polymer and its crystal structure is unprecedented for rare-earth succinates. It consists of centrosymmetric dimers of edge-sharing $HoO_7(H_2O)_2$ polyhedra linked by succinate ions in the [100] and [101] directions. Hydrogen-bonded hydration water molecules connect layers to give three-dimensional stability. Compound **2** is built up from infinite chains of $HoO_8(H_2O)$ polyhedra linked by succinates that result in a 3D architecture. This structure shows that hydrothermal conditions favor an increase in the overall dimensionality of these hybrids, in agreement with theoretical considerations. The compounds were characterized by FTIR and Raman spectroscopy, thermal analysis, and variable-temperature magnetic susceptibility measurements and the results are discussed in connection with the structural findings. The effect of the dimensionality on the thermal stability of both structures after removal of the hydration water molecules is also analyzed.

Introduction

The last few years have witnessed a great effort dedicated to the investigation, design, and prediction of open hybrid organic/inorganic frameworks with metal cations and multifunctional anions as structural agents.[1–8] Such molecular-based porous materials have potential utility in catalysis, optics, gas separation/storage, and host–guest chemistry.[9–14]

The observed wide use of dicarboxylates to build open framework systems is due to the versatility of these anions' interactions. Their different coordination modes with metals, many of which can coexist, and their ability to act as hydrogen-bond acceptors and donors make them capable of generating supramolecular assemblies and account for their multifunctionality. The synthesis of specific rare-earth dicarboxylates allows us to expand the range of applications of this kind of compounds by constructing smart materials with attractive optical or magnetic properties, depending on the nature of the metal ion.[15–17]

One important limitation for the practical application of hybrid materials is their thermal stability, although this can be considerably improved by the formation of extended metal–oxygen–metal arrays.[13] In the case of lanthanide dicarboxylates, the combination of lanthanide ions with a high coordination number and relatively flexible ligands, like aliphatic dicarboxylates, is expected to prevent collapse of the structure upon removal of guest molecules as well as interpenetration of networks, which obstructs the pores.

A large variety of coordination polymers have been synthesized by crystallization under mild conditions, and hydrothermal techniques allow the variety of structural types to be considerably extended. Although the synthesis conditions are known to play an important role in the framework dimensionality and hydration grade, the way in which all the variables influence the framework development is not yet clear. According to the literature, hydrothermal conditions are more suitable for preparing 3D solids with extended M–O–M networks, which favors better thermal stability since they enhance metal–ligand interactions rather

[a] Area de Química General e Inorgánica "Dr. G. F. Puelles", Facultad de Química, Bioquímica y Farmacia, Universidad Nacional de San Luis,
5700 San Luis, Argentina
E-mail: gnarda@unsl.edu.ar
[b] LANADI e IFLP, Departamento de Física, Facultad de Ciencias Exactas,
1900 La Plata, Argentina
[c] Facultad de Ingeniería, Universidad Nacional de La Plata, CC67,
1900 La Plata, Argentina
[d] Max-Planck-Institut für Kohlenforschung,
45470 Mülheim an der Ruhr, Germany

Supporting information for this article is available on the WWW under http://www.eurjic.org or from the author.

than metal–water coordination.[18,19] According to Férey et al.,[20] although helping the formation of M–O–M networks, hydrothermal conditions preclude the assistance of computer simulations in the rational design of this kind of compounds as hydrothermal conditions modify the nature of the species in solution.

Lanthanide succinates have been examined by various authors and several compounds have been reported in the literature, especially $[Ln_2(C_4H_4O_4)_3(H_2O)_2]$ (Ln = Ce,[21] Eu,[22] Gd[23] and Er;[24] type 1), $[Ln_2(C_4H_4O_4)_3(H_2O)_2]\cdot H_2O$ (Ln = Y, La,[14] Pr,[25] Sm,[21,25] Gd[23] and Tb;[22] type 2), and $[Lu_2(C_4H_4O_4)_3(H_2O)_4]\cdot 4H_2O$[26] (type 3). All of these have been obtained by hydrothermal synthesis or under high-temperature conditions and are 3D hybrid frameworks with channels that can host hydrogen-bonded hydration water molecules. Structural analyses have indicated that type-1 compounds, which crystallize in the triclinic system (space group $P\bar{1}$) and do not host hydration waters, present a framework with important structural similarities with type-2 compounds, which crystallize in the monoclinic $C2/c$ space group. Both structural types include infinite 1D inorganic networks (running along a crystallographic axis) that are built up from edge-sharing $LnO_8(H_2O)$ polyhedra interconnected by succinate dianions, with channels parallel to the chains. On the other hand, the lutetium succinate structure (type 3) consists of isolated, irregular $LuO_6(H_2O)_2$ polyhedra linked by organic moieties to form a three-dimensional framework.

To better understand the factors that influence the way of binding and the formation and stability of polymeric structures with different dimensionalities in hybrid systems we decided to explore the self-assembly of Ho^{III} and succinate ligands under ambient and hydrothermal conditions. Two novel dicarboxylate complexes, formulated as $[Ho_2(C_4H_4O_4)_3(H_2O)_4]\cdot 6H_2O$ (**1**) and $[Ho_2(C_4H_4O_4)_3(H_2O)_2]\cdot H_2O$ (**2**), were obtained and their thermal stability was studied. Their characterization by single-crystal X-ray diffraction, thermal and magnetic measurements, and FTIR and Raman spectroscopy are presented here. It is worth noting that the crystal structure of compound **1**, which was obtained under mild conditions, has not been observed previously and therefore it is the first lanthanide succinate with a 2D open structure.

Results and Discussion

Crystal Structures

Compound **1** crystallizes in the triclinic space group $P\bar{1}$ with $Z = 2$, although its structure is different from type 1 described above. Compound **2** crystallizes in the monoclinic space group $C2/c$ and is isostructural with all the Ln^{III} succinates that crystallize in the type-2 structure mentioned above (see Experimental Section).

There are two crystallographically independent anions in compound **1**. One (A) is located on an inversion center such that the anion has a perfect *trans* conformation (torsion angle: 180°) with a distance between the α and ω carbon atoms of 3.902(7) Å and the other anion (B) adopts a *gauche* conformation, with a torsion angle of –60.4(5)° and a distance between the α and ω carbon atoms of 2.999(7) Å. Both oxygens of both carboxylates of anion A are bound in a chelating mode, while although both O atoms of both carboxylates in anion B bind in a chelating mode, one oxygen atom of one of the carboxylates also acts in a bridging mode (see Scheme 1).

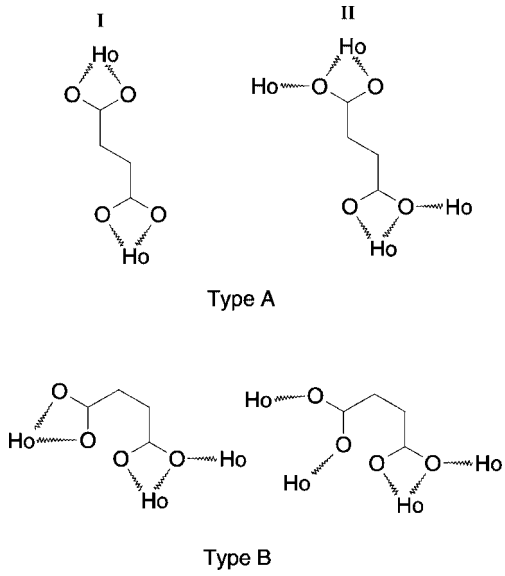

Scheme 1.

The Ho^{III} cations are coordinated by nine oxygen atoms, seven of them belonging to four succinate anions and the others to the two crystallographically inequivalent water molecules (Figure 1 and Table 1). The $HoO_7(H_2O)_2$ coordination polyhedra can be described as a monocapped square antiprism. Edge-sharing polyhedra, related by an inversion

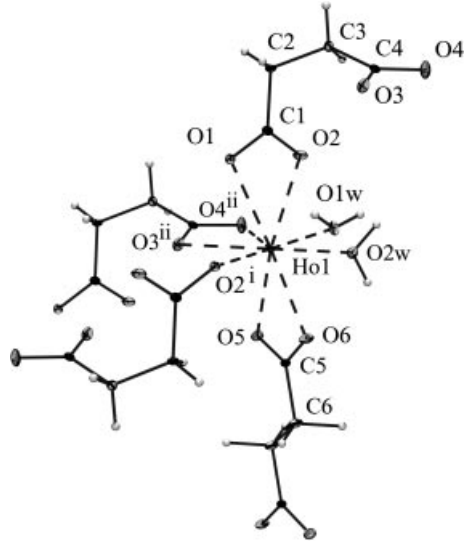

Figure 1. ORTEP-III view of the coordination polyhedron of Ho^{III} in **1** showing the atom-labeling scheme. Displacement ellipsoids are drawn at 50% probability. See footnote to Table 2 for symmetry codes.

Table 1. Selected intramolecular bond lengths [Å] and bond, torsion, and dihedral angles [°] for **1** and **2**. See footnote to Table 2 for symmetry codes.

Compound **1**					
Ho1–O1W	2.361(3)	C1–O2	1.280(5)	Ho1–O2–Ho1^{i}	112.4(1)
Ho1–O2W	2.317(3)	C1–C2	1.492(6)	O1–C1–C2–C3	–25.1(6)
Ho1–O1	2.419(3)	C2–C3	1.519(6)	O2–C1–C2–C3	155.5(4)
Ho1–O2	2.532(3)	C3–C4	1.500(6)	C1–C2–C3–C4	–60.4(5)
Ho1–O2^{i}	2.348(3)	C4–O3	1.272(5)	C2–C3–C4–O3	–24.4(6)
Ho1–O3^{ii}	2.399(3)	C4–O4	1.261(5)	C2–C3–C4–O4	157.7(4)
Ho1–O4^{ii}	2.459(3)	C5–O5	1.261(6)	O5–C5–C6–C6^{iii}	–177.1(5)
Ho1–O5	2.397(3)	C5–O6	1.269(6)	O6–C5–C6–C6^{iii}	3.1(8)
Ho1–O6	2.472(3)	C5–C6	1.504(6)	C5–C6–C6^{iv}–C5^{iv}	–180.0(4)
C1–O1	1.256(6)	C6–C6^{iii}	1.510(9)		
Compound **2**					
Ho1–O1W	2.434(5)	C1–C2	1.499(9)	C4–O4–Ho1^{x}	135.1(5)
Ho1–O1	2.497(5)	C2–C3	1.53(1)	O3–C4–O4	124.8(6)
Ho1–O1^{vi}	2.391(5)	C3–C4	1.516(8)	C4–O3–Ho1^{v}	145.0(4)
Ho1–O2	2.445(5)	C4–O3	1.247(8)	O1–C1–C2–C3	–68.5(7)
Ho1–O3^{v}	2.274(5)	C4–O4	1.265(9)	O2–C1–C2–C3	113.8(7)
Ho1–O4^{vii}	2.391(5)	C5–O5	1.281(8)	C1–C2–C3–C4	–73.1(8)
Ho1–O5	2.428(5)	C5–O6	1.495(10)	C2–C3–C4–O3	2.6(9)
Ho1–O5^{vi}	2.388(4)	C5–C6	1.495(11)	C2–C3–C4–O4	–178.0(6)
Ho1–O6	2.438(5)	C6–C6^{viii}	1.511(11)	O5–C5–C6–C6^{viii}	–176.2(8)
C1–O1	1.280(8)	Ho1^{ix}–O1–Ho1	110.1(2)	O6–C5–C6–C6^{viii}	1.8(12)
C1–O2	1.250(8)	Ho1^{ix}–O5–Ho1	112.6(2)	C5–C6–C6^{viii}–C5^{viii}	–180.0(6)
Plane P1: atoms:		Plane P2: atoms:		Plane P3: atoms:	
Ho, O1, Ho^{ii}, O1^{ii}		Ho, O1^{ii}, O2^{ii}		Ho, O1w, O3^{iii}, Ho^{ii}	
<P1,P2> = 17.5(2)°		<P2,P3> = 89.3(1)°			

center, form centrosymmetric dimers (see Figure 2) where the Ho^{III} cations are connected by two chelating bridging carboxylates, with the chelating plane (CP) departing 17.5(2)° from the bridging plane (BP; see Table 1 for plane labeling). These dimers are further strengthened by a hydrogen bond (HB) interaction involving the coordinated water W1 and the carboxylate oxygen O3 (see Table 2). The Ho···Ho distance within the dimer is 4.0579(2) Å. The distances between Ho^{III} and the coordinated succinate oxygen atoms range between 2.348(3) and 2.532(3) Å; these extreme values correspond to the bridging oxygen atoms O1 and O1^{ii} [O1–Ho–O1^{ii} angle: 112.4(1)°; ii: 1 – *x*, 1 – *y*, –*z*]. The overall structure can therefore be described as consisting of 2D organic–inorganic polymeric layers, as shown in Figure 3.

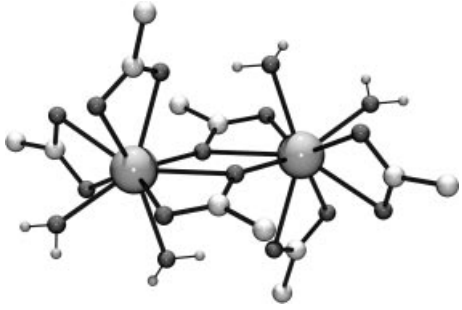

Figure 2. Perspective diagram showing the Ho^{III} and succinate ion connections in the dimer together with the bridging and chelating planes. For reasons of clarity only the relevant succinate fragments are shown. The Ho^{III} ions (bulky spheres) are medium color, while the carbon and oxygen atoms are light and dark gray, respectively.

Table 2. Hydrogen-bond interactions in **1** and **2**.[a]

	D–H [Å]	H···A [Å]	D···A [Å]	D–H···A [°]
Compound **1**				
O1W–H11W···O6^{ii}	0.777	2.141	2.790(5)	141.1
O1W–H12W···O3^{viii}	0.821	1.831	2.650(4)	175.1
O2W–H21W···O3W	0.924	1.829	2.719(5)	160.8
O2W–H22W···O5W	0.857	1.814	2.663(4)	170.1
O3W–H31W···O4W	0.850	2.212	2.852(5)	132.0
O3W–H32W···O5W^{xi}	0.849	2.125	2.809(5)	137.4
O4W–H41W···O4^{xii}	0.850	2.098	2.925(5)	164.4
O5W–H51W···O5^{xiii}	0.850	1.939	2.740(5)	156.5
O5W–H52W···O4W^{xiv}	0.850	2.185	2.694(6)	118.3
C6–H61···O4W^{xiii}	0.932	2.582	3.471(6)	159.6
C6–H62···O1W^{xiii}	1.149	2.519	3.449(5)	137.8
Compound **2**				
O1W–H11W···O4^{xv}	0.850	2.099	2.862(8)	149.1
O1W–H12W···O2^{v}	0.850	1.882	2.709(7)	164.2
O2W–H21W···O1W	0.998	2.129	2.939(8)	137.1
C2–H22···O6^{ix}	0.970	2.586	3.15(1)	117.6
C3–H31···O2W^{xiv}	0.970	2.575	3.51(2)	161.2
C6–H62···O2^{ix}	0.975	2.494	3.13(1)	122.7

[a] Symmetry codes: (i) –*x* + 1, – *y* + 1, –*z* + 2; (ii) *x* – 1, *y*, *z*; (iii) –*x*, –*y* + 1, –*z* + 1; (iv) 2 – *x*, 1 – *y*, 1 – *z*; (v) –*x* + 1/2, –*y* + 3/2, –*z* + 1; (vi) –*x* + 1/2, *y* + 1/2, –*z* + 1/2; (vii) *x*, –*y* + 1, *z* – 1/2; (viii) –*x*, 1 – *y*, –*z*; (ix) –*x* + 1/2, *y* – 1/2, –*z* + 1/2; (x) *x*, –*y* + 1, *z* + 1/2; (xi) 1 – *x*, –*y*, 1 – *z*; (xii) –*x*, –*y*, 1 – *z*; (xiii) 1 – *x*, 1 – *y*, 1 – *z*; (xiv) 1 + *x*, *y*, *z*; (xv) 1/2 – *x*, 1/2 – *y*, 1 – *z*.

Within a layer the dimers are connected by succinates A along [100] and succinates B along [101]. The connection along [100] is further stabilized by a HB between W1 and the succinate oxygen O5 (see Table 2). The hydration water molecules (W3, W4, and W5) are located between the 2D

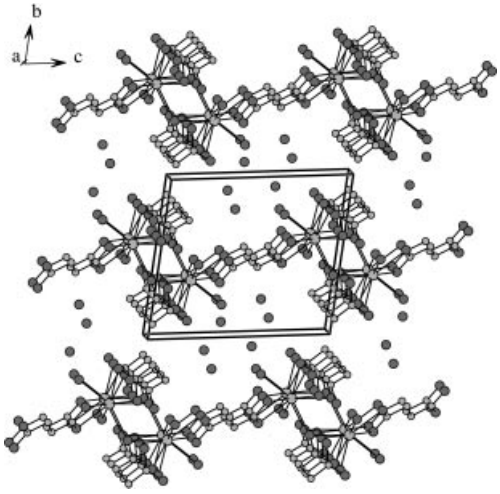

Figure 3. Projection of the framework along the *a* direction of **1**.

organic–inorganic polymeric layers. Hydration waters are connected by HBs to form six-membered clusters, which are located around the inversion centers at (0,0,1/2) and equivalent positions. The coordinated water W2 links clusters through two HBs, thus generating hydrogen-bonded chains of hydration water clusters running in the [100] direction. Hydration waters are further hydrogen bonded to succinate anions, providing in this way the connection between the layers and the stabilization of the three-dimensional arrangement. In spite of the differences in coordination number and coordination modes, we have observed a similar 2D structure in diaquasuccinatocadmium(II).[27,28]

There are also two crystallographically independent anions in compound **2**. One (A) is also located on an inversion center (perfect *trans* conformation) with a distance between the α and ω carbon atoms of 3.838(12) Å and the other (B) adopts a *gauche* conformation with a torsion angle of –73.1(8)° and a distance between the α and ω carbon atoms of 3.21(1) Å. Different to **1**, both carboxylates belonging to anion A in compound **2** coordinate the cations through a chelating and a bridging mode, while one carboxylate of anion B coordinates the cation through a chelating and a bridging mode and the two O atoms of the other carboxylate are only involved in a bridging interaction (see Scheme 1). The Ho^{III} cations in this compound are also coordinated to nine oxygen atoms, in this case adopting a tricapped trigonal prismatic geometry. In this structure just one oxygen of the coordination polyhedra belongs to a water molecule, with the other eight belong to six different carboxylate groups (see Figure 4 and Table 1). Neighboring Ho^{III} cations are connected by two chelating bridging carboxylates and by an additional bidentate carboxylate, which is oriented with the O–C–O plane almost perpendicular to the corresponding BP [the angle is 87.0(9)°; see Figure 5]. This connectivity, different from that observed in **1**, is extended by the twofold screw axis parallel to the *b* axis to build infinite chains where all Ho^{III} ions are at the same distance [4.007(1) Å]. In spite of this, bridging Ho–O–Ho geometries within adjacent polyhedra are different within three esd's. The bridging Ho–O distances are 2.391(5) and 2.388(4) Å [2.497(5) and 2.428(5) Å] and the Ho–O–Ho angle is 112.6(2)° [110.1(2)°; see Table 1]. The chains are connected by anions of type A running perpendicular to the (101) planes and by anions of type B situated along the [101] direction. Adjacent chains along *a* are 8.920(5) and 11.002(5) Å apart and those along *b* 6.016(7) and 7.894(6) Å apart. This arrangement helps the development of an open-framework with two set of channels of different cross-section size [28.8(5) and 20.8(5) $Å^2$], both of which run parallel to the HoO_2 chains with the hydration waters located in the largest channel, as can be seen in Figure 6. The hydration waters are linked to the framework by hydrogen bonds (see Table 2). They interact as donors with coordination waters and as H-acceptors from type-B succinate anions.

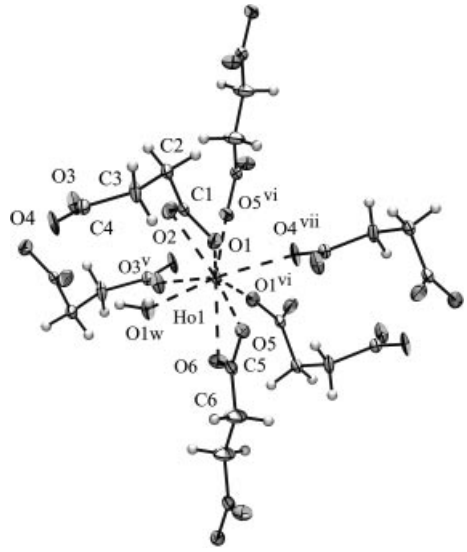

Figure 4. ORTEP-III view of the coordination polyhedron of Ho^{III} in **2** showing the atom-labeling scheme. Displacement ellipsoids are drawn at 50% probability. See footnote to Table 2 for symmetry codes.

Figure 5. Perspective diagram showing the Ho^{III} and succinate ion connections along the chain together with the bridging and chelating planes. Similar to Figure 2, the relevant succinate fragments and gray shades are used.

Taking into account the synthesis conditions that give rise to each structure, it can be inferred that the presence of a higher number of coordination waters, the smaller Ho–OW distances, and the less rich coordination modes of the dicarboxylate anions in **1** are favored by the milder conditions of the solution. This synthesis path leads to the devel-

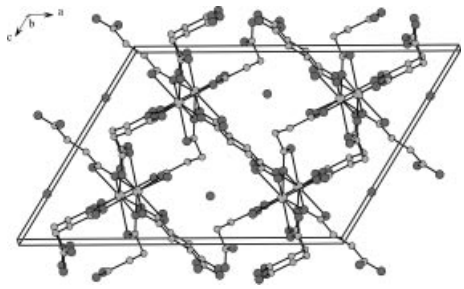

Figure 6. Projection of the framework along the *b* direction of **2**.

opment of 2D organic–inorganic polymeric layers whose hydrophilic surfaces are linked by the hydration waters. On the other hand, the hydrothermal conditions used for the synthesis of **2** help to prevent the presence of a high number of coordination waters and enhance carboxylate coordination, thereby facilitating the formation of infinite Ho–O–Ho networks (see Figure 5) and a 3D framework structure. A comparison of the densities reported in Table 3 shows that they increase with the temperature employed during the synthesis. This correlates with the increasing dimensionality and is in accordance with the results reported in the literature for other metal dicarboxylates.[18,19,29]

Vibrational Spectra

Figure 7 shows the FTIR and Raman spectra of both compounds. IR and Raman frequencies values for compound **2** are reported in parentheses below. The interpretation of the IR and Raman spectra is performed by considering the internal vibrations of water molecules, carboxylates, and methylene groups and their comparison with those observed in succinic acid and other related compounds. According to structural data, both structures are centrosymmetric ($P\bar{1}$ and $C2/c$) and no coincidences between IR and Raman frequencies (or at least only a few) can be expected, in agreement with the mutual exclusion rule.

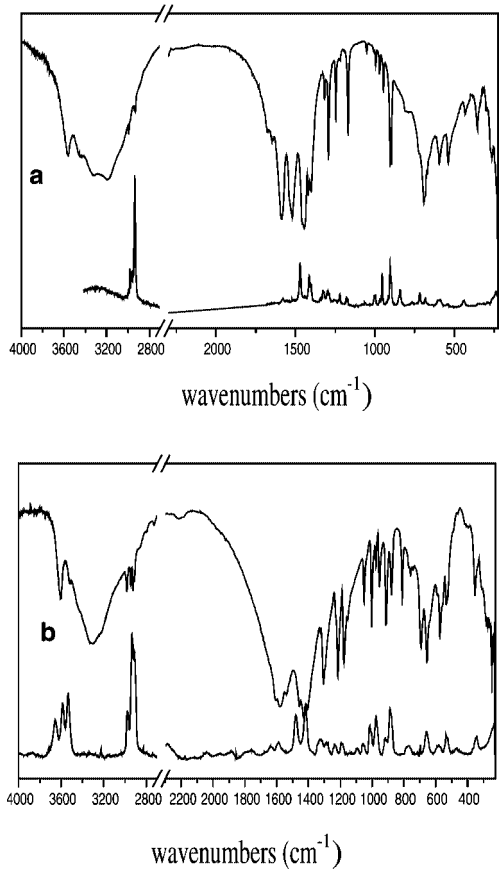

Figure 7. FTIR (top) and Raman (bottom) spectra of a) **1** and b) **2**.

Water Modes

The assignment of these modes, particularly the librational ones, was performed by comparing the spectra of partially and completely dehydrated samples, which were obtained by using a variable-temperature IR cell (the thermal diagrams were taken into account; see Figure 8).

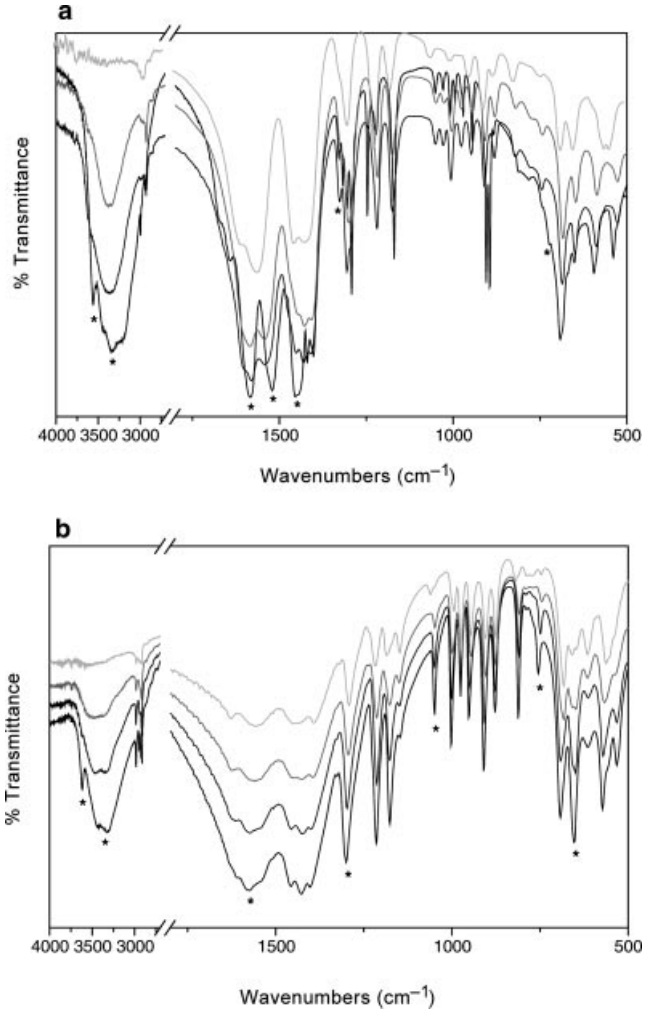

Figure 8. FTIR spectra recorded as a function of temperature during the dehydration of a) **1** and b) **2**. The most notable changes are indicated with asterisks.

The ν(OH) absorption can be identified in the FTIR spectrum of compound **1** as one broad, markedly asymmetric band that involves several components. This fact is consistent with the structural data, where four different kinds

of water molecules are seen to be present. The components centered at 3560 and 3460 cm^{-1} (3560, 3520, and 3445 cm^{-1} for **2**) are mainly associated with hydration water since they disappear after partial dehydration; on the contrary, those centered at 3330 and 3175 cm^{-1} (3315 and 3210 cm^{-1} for **2**), which are absent upon complete dehydration, can be attributed to the remaining coordinated water.

The two low-intensity bands located at 1675 and 1645 cm^{-1} are associated with the bending mode; the former is related to those water molecules that are eliminated first during thermal treatment since it is absent in the spectra of partially dehydrated samples.

OCO Group Modes

Both carboxylate stretching modes are present in the FTIR spectra as broad, asymmetric bands with various components included. The splitting of these modes can be explained in terms of the different types of interactions between the carboxylate groups and the Ho^{III} cations found in the crystals of both compounds (see Scheme 1). Two bands at 1585 and 1520 cm^{-1} (1610, 1580, and 1540 cm^{-1}) are assigned to ν_{as}(OCO), with the bands at 1330, 1315, and 1305 cm^{-1} (1300 cm^{-1}) being associated with the corresponding symmetric mode. Splitting of the OCO stretching modes is not observed in the IR spectra of metal succinates where a unique binding mode for carboxylate groups has been reported.[28,30] No evidence for a carbonyl absorption is present, in agreement with the observed C–O distances (see Table 1).

Thermal Analysis

TGA curves and thermodiffractograms up to complete dehydration for compounds **1** and **2** are shown in Figures 9 and 10, respectively. The temperature values were selected with reference to TG and *d*TG data; experimental Δm percentages and temperature values for compound **2** are presented in parentheses. The differences between the Δm percentages found for both compounds and the calculated ones do not exceed 1%. Dehydration proceeds in two stages at 68 °C (55 °C) and 115 °C (176 °C), as expected from the structural data. The first weight loss of 12.5% (1.93%) is related to loss of hydration water whereas the second mass decay of 8% (4.97%) corresponds to the elimination of coordinated water molecules. Differential water removal has also been observed in other type-2 lanthanide succinates, such as the La and Gd ones, whereas in those of Y, Pr, Sm, and Tb hydration and coordinated water molecules are lost in a single step.

A comparison of the dehydration events in **1** and **2** highlights noticeable differences. The continuous loss of weight between 40 and 87 °C for compound **1** accounts for the different interactions of the clustered hydration water molecules, and a rather narrow range of temperatures separates it from the next dehydration step. On the contrary, compound **2** exhibits an extended plateau of stability in the range 60–150 °C after hydration water elimination. These differences in the thermal behaviors of **1** and **2** can be explained as a consequence of the hydrogen bonds inside the framework and the interactions with the water molecules in the channels. These results show that the hydration water in **2** is looser than in other type-2 compounds such as that of

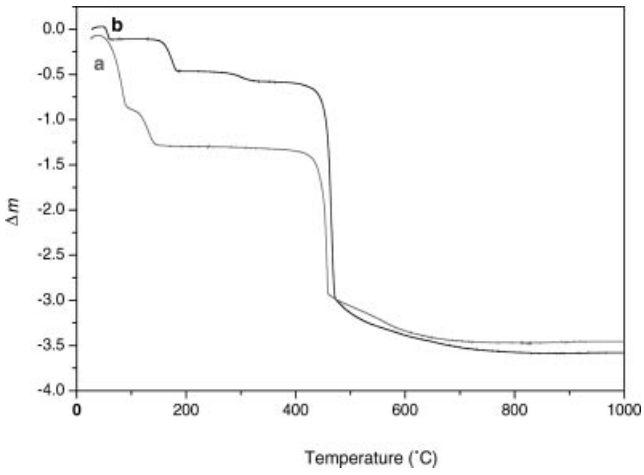

Figure 9. TG curves of **1** and **2**.

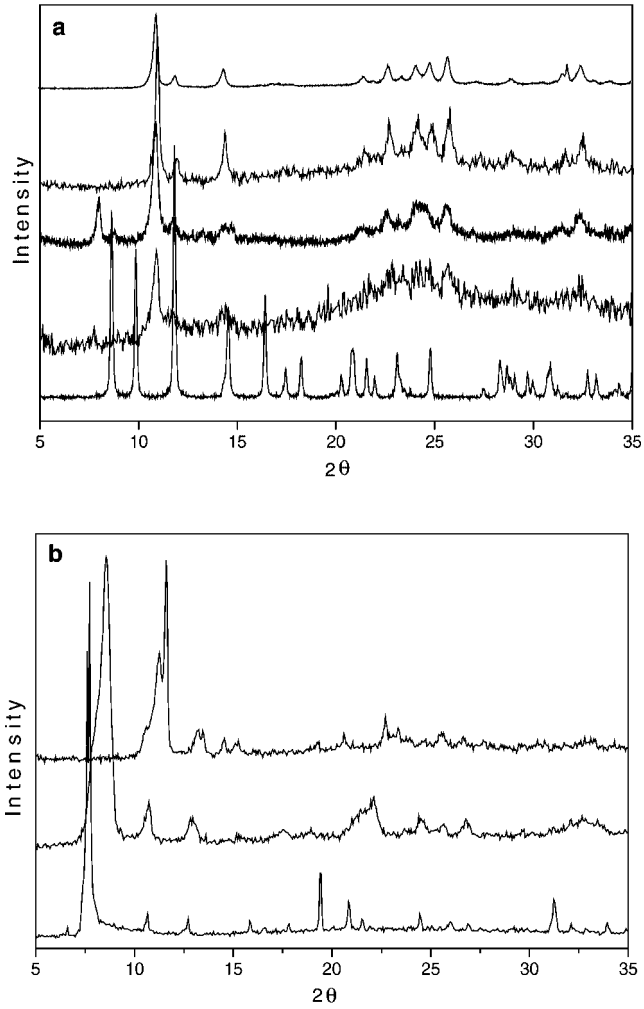

Figure 10. XRD patterns as a function of temperature of a) **1** and b) **2** thermolyzed to dehydration.

Sm^{III}, where the DTA curve only shows one peak at 214 °C due to loss of both hydration and coordinated waters, or Gd^{III}, where lattice and coordinated water molecules are lost in the 200–240 °C and 270–325 °C ranges, respectively.

Dehydration of compounds **1** and **2** was also followed by variable-temperature FTIR spectroscopy (Figure 8). The broad band assigned to the ν(OH) stretching gradually decreases in intensity until its complete disappearance at higher temperature. The OCO stretching bands are strongly affected by dehydration of compound **1** due to the progressive degradation of the H-bond network. Thermally induced changes in these modes are less significant for compound **2**, where a shift to lower frequencies is observed in the main component of the ν_{as}(OCO) and in the corresponding ν_s(OCO) band. The spectra recorded at the highest temperature for both compounds do not display the librational modes of water molecules below 1100 cm^{-1}.

The removal of hydration water molecules in **1** leads to an amorphous phase that recrystallizes on further heating and remains stable, with increasing crystallinity, up to succinate ion decomposition, as has been observed for other 2D metallic dicarboxylates (see Figure 10a).[27,30] An extremely weak endothermic DSC signal at 165 °C is related to this transition (see Supporting Information). The X-ray powder diffraction pattern of the new crystalline phase, corresponding to the anhydrous compound, was indexed in the monoclinic space group *P*2/*m* (no. 10), using the TREOR program,[31] with the following cell parameters: a = 19.378(5), b = 8.157(4), c = 4.236(1) Å, and β = 92.22(1)°. Taking into account the structural features of compound **1** (described above), it is reasonable to expect that removal of hydration water implies loss of crystallinity.

Compound **2** essentially retains its crystalline structure when the first water molecule is lost, with the decrease in the XRPD intensity being the most outstanding difference between patterns corresponding to different temperature treatments (see Figure 10b).

The thermal evolution of both compounds presents a final event at 442 °C for **1** (460 °C for **2**) which is associated with succinate ion decomposition to give cubic holmium oxide as the final product; this is stable up to 1000 °C (PDF card 43-1018). A change in the slope of the TG trace around 500 °C suggests the formation of an intermediate product. A carbonated phase, which further decomposes to the oxide, appears upon heating to 500 °C and its identification was performed by FTIR spectroscopy, which exhibits characteristic bands at 1390 and 860 cm^{-1}.[32]

Magnetic Measurements

The magnetic behavior of **1** and **2** is shown in Figure 11, where the real component of the AC magnetic susceptibility (χ') and the product $\chi'T$ are plotted against temperature. In both cases, at temperatures below 100 K, the $\chi'T$ curve departs from a Curie–Weiss law. The Curie constant, C, and Curie temperature, θ, were determined from a linear fit of the inverse of χ'^{-1} in the range of temperatures where the Curie–Weiss law stands. This fit yields the values C = 14.27(7) and 13.49(3) $cm^3\,K\,mol^{-1}$ and θ = –2.5(5) and –3.6(6) K for **1** and **2**, respectively. The negative value of the Curie temperature and the temperature dependence of $\chi'T$ indicate that an antiferromagnetic ordering is reached at lower temperatures. The effective magnetic moments (μ_{eff}) calculated from the Curie constants are 10.68(1) μ_B for **1** and 10.37(1) μ_B for **2**, both of which are very close to the effective magnetic moment of the free Ho^{III} cation (10.6 μ_B). The observed lower μ_{eff} value in **2** might be a consequence of the higher delocalization of the Ho^{III} electrons in this compound due to the higher number of oxy-

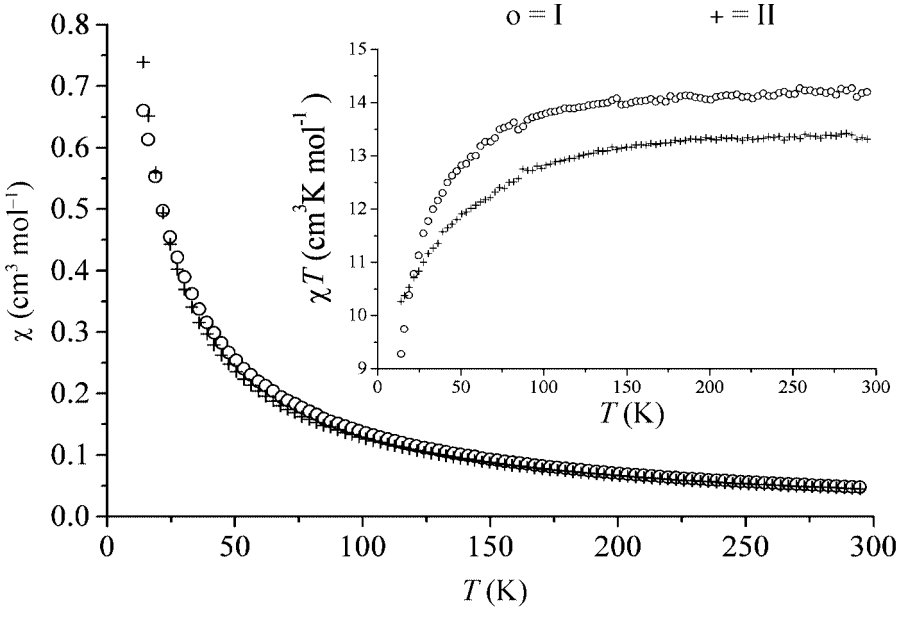

Figure 11. Thermal dependence of χ' for **1** and **2**. The inset shows the $\chi'T$ curves, which display the Curie–Weiss antiferromagnetic behavior of both compounds.

gens belonging to succinate anions in the coordination sphere.

At low temperatures, where the $\chi' T$ curves deviate from the Curie–Weiss law, the calculated μ_{eff} values at 14 K are 8.62(4) μ_B for **1** and 9.06(1) μ_B for **2**. A deviation of the magnetic behavior from a Curie–Weiss law and a decrease of the $\chi' T$ product with temperature have been observed in other Ho^{III} carboxylates[33] and have been mainly ascribed to crystal field effects, which induce a depopulation of the rare-earth cation Stark components at low temperatures.

Conclusions

Two Ho^{III} succinate coordination polymers, namely $[Ho_2(C_4H_4O_4)_3(H_2O)_4]\cdot 6H_2O$ (**1**) and $[Ho_2(C_4H_4O_4)_3(H_2O)_2]\cdot H_2O$ (**2**), have been prepared and characterized employing mild and hydrothermal conditions, respectively. Ho^{III} is nine-coordinate in both compounds. The structure of **1** consists of 2D organic–inorganic polymeric layers where coordination polyhedra form dimers that are connected by hydrogen-bonded hydration waters. In **2**, neighboring Ho^{III} ions build infinite Ho–O–Ho chains linked by *trans* and *gauche* succinates. Chain formation supports the development of a hybrid open framework with two set of channels of different size, the largest of which contains the hydration waters. Thus, the multidentate character of the succinate ions in this compound, together with the substitution of a water ligand by an oxygen of the OCO groups, favors the formation of infinite M–O–M networks and plays an important role in the inorganic condensation. This also allows us to explain the observed difference in the magnetic results as being due to the presence of a dissimilar number of oxygens belonging to the succinate anions in the coordination sphere.

A crystalline anhydrous phase is obtained upon heating **1** after water removal, while the partially dehydrated compound obtained upon heating **2** shows a plateau of thermal stability, which indicates the potential capability of the dehydrated form of **2** to act as a stable open-framework material with empty channels.

All the above results show the effect of the synthesis conditions on the dimensionality and thermal stability of the metal-organic polymers and reinforce the necessity of the hydrothermal method for the formation of inorganic networks and open channels. However, other parameters, at present under study, need to be looked at to understand the relationship between synthesis temperature and the structure and properties of the products.

Experimental Section

Synthesis: Reagents of analytical grade were used in the synthesis of compounds **1** and **2** according to the following procedures.

$[Ho_2(C_4H_4O_4)_3(H_2O)_4]\cdot 6H_2O$ (1): $HoCl_3\cdot 6H_2O$ (2 mmol) was dissolved in distilled water (100 mL) and then added to an aqueous solution containing succinic acid (3 mmol, 100 mL) whilst stirring; the resulting pH was raised to 4.5 by NaOH addition. The solution was then left to evaporate slowly at room temperature. A large number of pale-orange, needle-shaped single crystals (70% yield) suitable for a crystallographic study were obtained after several days. These were filtered, washed with distilled water, and dried at room temperature. $C_6H_{16}HoO_{11}$ (429.12): calcd. C 16.39, H 3.81; found C 16.78, H 3.73.

$[Ho_2(C_4H_4O_4)_3(H_2O)_2]\cdot H_2O$ (2): A solution prepared as described above (50 mL) was allowed to react under autogenous pressure for 3 d at 180 °C. Pale-orange, prismatic single crystals (58% yield) suitable for a crystallographic study were obtained. These were filtered, washed with distilled water, and dried at room temperature. $C_6H_{10}HoO_{7.5}$ (367.07): calcd. C 19.71, H 2.58; found C 19.63, H 2.45.

X-ray Powder Diffraction (XRPD): X-ray powder diagrams were obtained with a Rigaku D-MAX-IIIC diffractometer using Cu-K_α radiation (Ni filter) and NaCl and quartz as external calibration standards.

Single-Crystal Structure Determination: Single-crystal X-ray data for compound **1** were collected using a KappaCCD area detector diffractometer equipped with a Bruker AXS FR591 rotating anode. Data collection and determination of the unit cell parameters were performed with the Nonius collect software package, while integration of the data frames and scaling of the intensities were performed using the DENZO suite of programs.[34] Room temperature data did not provide a flat difference-Fourier synthesis map, proba-

Table 3. Crystal data, structure determination, and refinement summary for $[Ho_2(C_4H_4O_4)_3(H_2O)_4]\cdot 6H_2O$ (**1**) and $[Ho_2(C_4H_4O_4)_3(H_2O)_2]\cdot H_2O$ (**2**).

	1	**2**
Crystal system	triclinic	monoclinic
Empirical formula	$C_6H_{16}HoO_{11}$	$C_6H_{10}HoO_{7.5}$
Formula mass	429.12	367.07
Space group	$P\bar{1}$	$C2/c$
a [Å]	6.49590(10)	19.899(2)
b [Å]	9.6737(2)	7.681(2)
c [Å]	10.4356(2)	13.813(2)
α [°]	79.5780(10)	90
β [°]	89.7050(10)	121.534(10)
γ [°]	70.8820(10)	90
V [Å^3]	608.34(2)	1799.5(6)
$\rho_{calcd.}$ [g cm^{-3}]	2.343	2.710
Z	2	8
$F(000)$	414	1376
μ (Mo-K_α/Cu-K_α) [mm^{-1}]	6.554	16.683
Crystal size [mm]	0.14 × 0.08 × 0.04	0.40 × 0.03 × 0.02
T_{min}/T_{max}	0.259/0.596	0.133/0.613
Temperature [K]	100(1)	293(2)
λ (Mo-K_α/Cu-K_α) [Å]	0.71073	1.54184
Monochromator	graphite	graphite
θ range for data collection [°]	3.29 to 31.02	5.22 to 67.91
Completeness to θ = 31.02/67.91°	99.8%	94.2%
Limiting indices	$-9 \le h \le 9$	$-23 \le h \le 20$
	$-14 \le k \le 14$	$-1 \le k \le 9$
	$-15 \le l \le 15$	$0 \le l \le 16$
Reflections collected/unique with $I > 2\sigma(I)$	14505/3872	1886/1538
Refined parameters	164	136
Goodness-of-fit on F^2	1.236	0.956
R	0.0278	0.0603
R_w	0.1210	0.1739
$(\Delta/\rho)_{max}/(\Delta/\rho)_{min}$ [e Å^{-3}]	2.313/–3.685	2.146/–2.339

bly due to thermal smearing induced by motion of the hydration waters. The crystal was therefore cooled down to 100 K in a stream of cold nitrogen gas using a Cryostream cooler from Oxford Cryosystems. Data collected at that temperature were used for structure refinement. Data for compound **2** were collected on an automatic four-circle CAD-4 diffractometer at ambient temperature (293 K). CAD-4 software was used for data collection and cell refinement.[35] The program XCAD4[36] was employed for data reduction. Both structures were solved by direct methods using SHELXS-86[37] and refined by full-matrix least-squares based on F^2 using SHELXL-93.[38] The succinate hydrogen atoms in both structures were located from a difference-Fourier synthesis, while the program CALC-OH[39] was employed to calculate the position of the hydrogen atoms of water. Further refinements were performed with the hydrogen atoms riding on bound atoms. The structural analyses were performed with PLATON[40] and PARST.[41] The molecular graphics were produced with ORTEP[42] and POV-Ray.[43] Crystal data and details of data collection and structure refinement are given in Table 3. Selected interatomic distances and bond, torsion, and dihedral angles are listed in Table 1. Table 2 lists the H-bonds' geometry.

CCDC-618378 and -618379 contain the supplementary crystallographic data for this paper. These data can be obtained free of charge from The Cambridge Crystallographic Data Center via www.ccdc.cam.ac.uk/data_request/cif.

Infrared and Raman Spectroscopy: FTIR spectra were recorded with a Nicolet Protégé 460 spectrometer in the 4000–225 cm^{-1} range with 32 scans, using the KBr pellet technique; spectral resolution was 4 cm^{-1}. Raman spectra were recorded with a Raman Jobin–Yvon T64000 equipped with a CCD and an Ar laser operating at 514.5 nm.

Thermal Analysis: TG curves and DSC measurements were recorded with a Shimadzu TGA-50H thermal analyzer apparatus and a Shimadzu DSC-60 apparatus under flowing oxygen at 50 mL min^{-1} at a heating rate of 10 °C min^{-1}. Appropriate combinations of X-ray powder diffraction and FTIR spectroscopy were used for further characterization of the pyrolysis products.

Magnetic Measurements: Magnetic measurements were carried out in the range 14–330 K with a LakeShore 7130 AC Susceptometer with an alternating field of 1 Oe and 825 Hz.

Supporting Information (see footnote on the first page of this article): DSC diagram of compound **1** to support the thermal analysis.

Acknowledgments

The authors thank the Consejo Nacional de Investigaciones Científicas y Técnicas (CONICET: PID 4929 and PID 6007), the Agencia Nacional de Promoción Científica y Tecnológica (PICT 03041), the Comisión de Investigaciones Científicas de la Provincia de Buenos Aires (CICPBA), Universidad Nacional de La Plata (UNLP), Universidad Nacional de San Luis (UNSL), Republica Argentina and Consejo Superior de Investigaciones Científicas (CSIC), Spain, for financial support. Dr. A. P. Ayala is acknowledged for his assistance in measuring the Raman spectra. The authors are grateful to the Comisión Nacional de Energía Atómica (CNEA) for providing the TXRD equipment. G. P., G. E. E., and G. E. N. are members of the CONICET. C. G. P. and M. C. B. acknowledge a CONICET fellowship.

[1] B. F. Abrahams, V. Hoskins, D. M. Michail, R. Robson, *Nature* **1994**, *369*, 727.
[2] M. L. MacGillavray, S. Subramanian, M. J. Zaworotko, *J. Chem. Soc., Chem. Commun.* **1994**, 1325.
[3] A. K. Cheetham, G. Férey, T. Loiseau, *Angew. Chem. Int. Ed.* **1999**, *38*, 3268.
[4] C. N. R. Rao, S. Natarajan, R. Vaidhyanathan, *Angew. Chem. Int. Ed.* **2004**, *43*, 1466.
[5] R. Vaidhyanathan, S. Natarajan, C. N. R. Rao, *Dalton Trans.* **2003**, 1459.
[6] G. Férey, *Chem. Mater.* **2001**, *13*, 3084.
[7] G. Shimizu, *J. Solid State Chem.* **2005**, *178*, 2519.
[8] P. M. Forster, A. K. Cheetham, *Top. Catal.* **2003**, *24*, 79.
[9] O. M. Yaghi, G. Li, H. Li, *Nature* **1995**, *378*, 703.
[10] N. L. Rosi, M. Eddaudi, J. Kim, M. O'Keefe, O. M. Yaghi, *CrystEngComm* **2002**, *4*, 401.
[11] R. Eberhardt, M. Allmendinger, M. Zintl, C. Troll, G. Luinstra, B. Rieger, *Macromol. Chem. Phys.* **2004**, *205*, 42.
[12] M. Eddaoudi, H. Li, T. Reineke, M. Fehr, D. Kelley, T. Groy, O. M. Yaghi, *Top. Catal.* **1999**, *9*, 105.
[13] P. M. Forster, A. K. Cheetham, *Angew. Chem. Int. Ed.* **2002**, *41*, 457.
[14] J. Perles, M. Iglesias, C. Ruiz-Valero, N. Snejko, *J. Mater. Chem.* **2004**, *14*, 2683.
[15] J. Legendziewicz, B. Keller, I. Turowska-Tyrk, W. Wojciechowski, *New J. Chem.* **1999**, *23*, 1097.
[16] Y. Kim, M. Suh, D.-Y. Jung, *Inorg. Chem.* **2004**, *43*, 245.
[17] R. Hill, D.-L. Long, P. Hubberstey, M. Schröder, N. Champness, *J. Solid State Chem.* **2005**, *178*, 2414.
[18] C. Livage, C. Egger, G. Férey, *Chem. Mater.* **2001**, *13*, 410.
[19] P. M. Forster, A. Burbank, C. Livage, G. Férey, A. K. Cheetham, *Chem. Commun.* **2004**, 368.
[20] G. Férey, C. Mellot-Draznieks, C. Serre, F. Millange, *Acc. Chem. Res.* **2005**, *38*, 217.
[21] A. Seguatni, M. Fakhfakh, M. Vauley, N. Jouini, *J. Solid State Chem.* **2004**, *177*, 3402.
[22] G.-H. Cui, J.-R. Li, R.-H. Zhang, X.-H. Bu, *J. Mol. Struct.* **2005**, *740*, 187.
[23] Y.-F. Zhou, F.-L. Jiang, D.-Q. Yuan, B.-L. Wu, M.-C. Hong, *J. Mol. Struct.* **2005**, *743*, 21.
[24] G.-Y. Dong, G.-H. Cui, J. Lin, *Acta Crystallogr., Sect. E* **2006**, *62*, 738.
[25] F. Serpaggi, G. Férey, *Microporous Mesoporous Mater.* **1999**, *32*, 311.
[26] M. Fleck, *Z. Kristallogr.* **2002**, *NCS 217*, 569.
[27] E. V. Brusau, J. C. Pedregosa, G. Echeverría, G. Punte, G. E. Narda, *J. Solid State Chem.* **2000**, *153*, 1.
[28] E. V. Brusau, J. C. Pedregosa, G. Echeverría, G. Pozzi, G. Punte, G. E. Narda, *J. Coord. Chem.* **2001**, *54*, 469.
[29] L. A. Borkowski, C. L. Cahill, *Inorg. Chem. Commun.* **2004**, *7*, 725.
[30] Y. J. Kim, D.-Y. Jung, *Inorg. Chem.* **2000**, *39*, 1470.
[31] P. E. Werner, L. Eriksson, M. Westdahl, *J. Appl. Crystallogr.* **1985**, *18*, 367.
[32] K. Nakamoto, *Infrared and Raman Spectra of Inorganic and Coordination Compounds*, 5th ed., John Wiley & Sons, Inc., USA, **1997**, 182.
[33] R. Baggio, M. T. Garland, O. Peña, M. Perec, *Inorg. Chim. Acta* **2005**, *358*, 2332.
[34] Z. Otwinowski, W. Minor, "Processing of X-ray Diffraction Data Collected, in Oscillation Mode", *Methods in Enzymology*, vol. 276: Macromolecular Crystallography, part A, p. 326 (Eds.: C. W. Carter Jr., R. M. Sweet), Academic Press, New York, **1997**, 307.
[35] CAD4 Express Software, Enraf–Nonius, Delft, The Netherlands, **1994**.
[36] K. Harms, S. Wocadlo, *XCAD-4*, *Program for Processing CAD-4 Diffractometer Data*, University of Marburg, Germany, **1995**.

[37] G. M. Sheldrick, *SHELXS86, Program for Crystal Structure Solution*, Institut für Anorganische Chemie der Universität, Tammannstrasse 4, Göttingen, Germany, **1986**.
[38] G. M. Sheldrick, *SHELXL93, Program for the Refinement of Crystal Structures*, University of Göttingen, Göttingen, Germany, **1993**.
[39] M. Nardelli, *J. Appl. Crystallogr.* **1999**, *32*, 563.
[40] A. L. Spek, *Acta Crystallogr., Sect. A* **1990**, *46*, C34.
[41] PARST: M. Nardelli, *J. Appl. Crystallogr.* **1995**, *28*, 659.
[42] M. N. Burnett, C. K. Johnson, *ORTEP-III Report ORNL-6895*, Oak Ridge National Laboratory, Oak Ridge, Tennessee, U. S. A., **1996**.
[43] C. J. Cason, *Persistence of Vision Ray Tracer* (POV-Ray™), Version 3.1e.watcom.win32 (optimized for Pentium® II processor), **1999**.

Received: September 14, 2006
Published Online: January 4, 2007

